LBL-35166
UC-600

Lawrence Berkeley Laboratory
UNIVERSITY OF CALIFORNIA

EARTH SCIENCES DIVISION

Presented at the International Workshop on
Research and Development of Geological Disposal,
Tokai, Japan, November 15–19, 1993, and to be
published in the Proceedings

Overview of Medium Heterogeneity and Transport Processes

Y. Tsang and C.-F. Tsang

November 1993

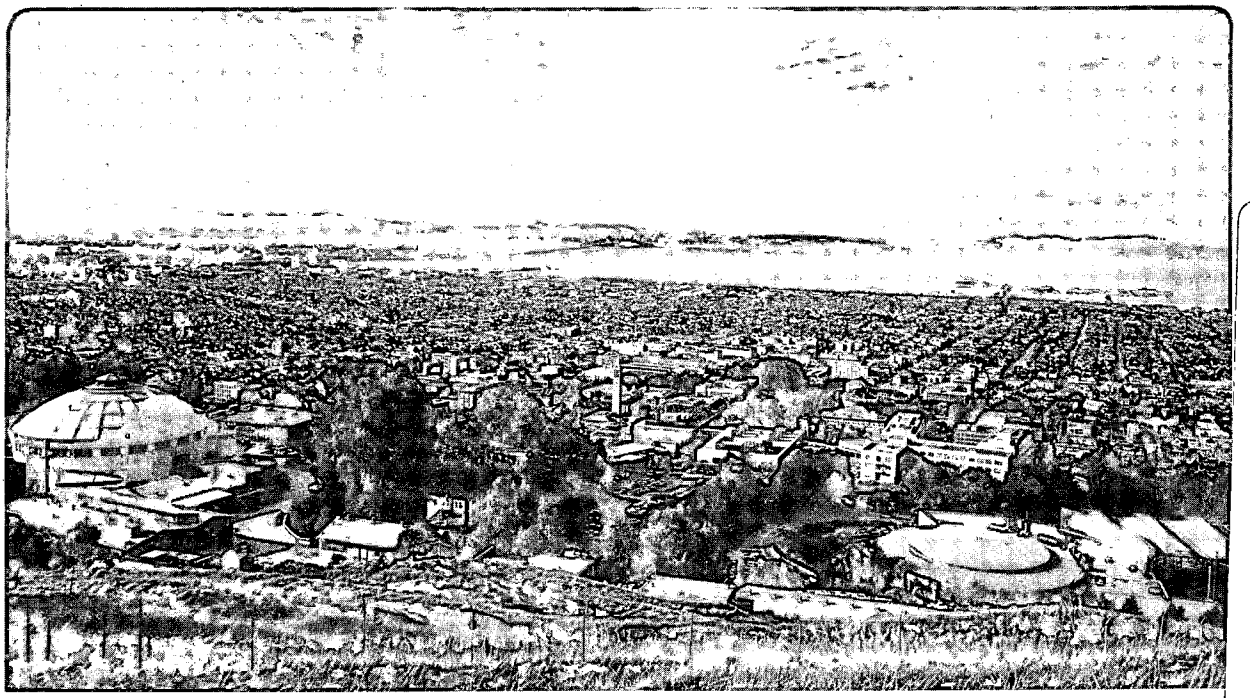

Prepared for the U.S. Department of Energy under Contract Number DE-AC03-76SF00098

DISCLAIMER

LBL-35166
UC-600

Overview of Medium Heterogeneity and Transport Processes

Y. Tsang and C.-F. Tsang

Earth Sciences Division
Lawrence Berkeley Laboratory
University of California
Berkeley, California 94720

November 1993

This work was jointly supported by the Swedish Nuclear Power Inspectorate (SKI) of Sweden and the Power Reactor and the Nuclear Fuel Development Corporation (PNC) of Japan. The latter support is through the DOE-PNC Binational Cooperative Agreement, PNC-LBL Annex, under the auspices of the U.S. Department of Energy Contract No. DE-AC03-76SF00098.

Overview of Medium Heterogeneity and Transport Processes

Yvonne Tsang[1] and Chin-Fu Tsang[2]

Introduction

Medium heterogeneity can have significant impact on the behavior of solute transport (Tsang and Tsang, 1989). Tracer breakthrough curves from transport in a heterogeneous medium are distinctly different from that in a homogeneous porous medium. Usually the shape of the breakthrough curves are highly non-symmetrical with a fast rise at early times and very long tail at late times, and often, they consist of multiple peaks. Moreover, unlike transport in a homogeneous medium where the same transport parameters describe the entire medium, transport through heterogeneous media gives rise to breakthrough curves which have strong spatial dependence. These inherent characteristics of transport in heterogeneous medium present special challenge to the performance assessment of a potential high level nuclear waste repository with respect to the possible release of radio nuclides to the accessible environment. Since an inherently desirable site characteristic for a waste repository is that flow and transport should be slow, then transport measurements in site characterization efforts will necessarily be spatially small and temporally short compare to the scales which are of relevance to performance assessment predictions. How feasible then is the extrapolation of results from site characterization to predictions for performance assessment?

In this paper we discuss the role of medium heterogeneity in site characterization and performance assessment. Our discussion will be based on a specific example of a 3D heterogeneous stochastic model of a site generally similar to the Äspö Island, the site of the Hard Rock Laboratory in Southern Sweden. For our study, alternative 3D stochastic fields of hydraulic conductivities conditioned on "point" measurements shall be generated. Results of stochastic flow and transport simulations would be used to address the issues of: (1) the relationship of tracer breakthrough with the structure of heterogeneity, and (2) the inference from small scale testing results to large scale and long term predictions.

Stochastic Flow and Transport Model

Site investigation measurements such as those carried out in Äspö result in a wealth of geological, physical and hydrological data. Our stochastic model relies mostly on hydrologic data. The fractured-porous medium of the site is represented by a 3D stochastic field of variable hydraulic conductivities. The generated 3D random field is

---

[1] Group Leader, Site characterization, Nuclear Waste Disposal Department, Earth Sciences Division, Lawrence Berkeley Laboratory, 1 Cyclotron Road, Berkeley, California, 94720, USA.
[2] Head, Environmental Remediation Technology Department, Earth Sciences Division, Earth Sciences Division, Lawrence Berkeley Laboratory, 1 Cyclotron Road, Berkeley, California, 94720, USA.

conditioned on the "point" measurements based on injection tests in 3 m packed sections, available from seven boreholes ranging from 600-1000m in depth. Figure 1 shows the frequency distribution of the measured hydraulic conductivity values. For the generation of 3D stochastic hydraulic conductivities, the non-parametric, conditioned, multiple indicator simulator ISIM3D (Gómez-Hernandez and Srivastava, 1990) is used. The non-parametric technique allows us to input the distribution "as is" given by the data shown in Figure 1 and not requiring a fit by a parametric distribution such as a log normal distribution. The indicator random variable $Z(\mathbf{x})$ at location $\mathbf{x}$ and for threshold z_o is defined by the following binary transform:

$$I(x;z_o)=\begin{cases}0 & Z(x)>z_o\\ 1 & Z(x)\le z_o\end{cases}, \qquad (1)$$

The expected value of $I(x,z_o)$ is

$$E\{I(x;z_o)\}=P\{Z(x)\le z_o\} \quad . \qquad (2)$$

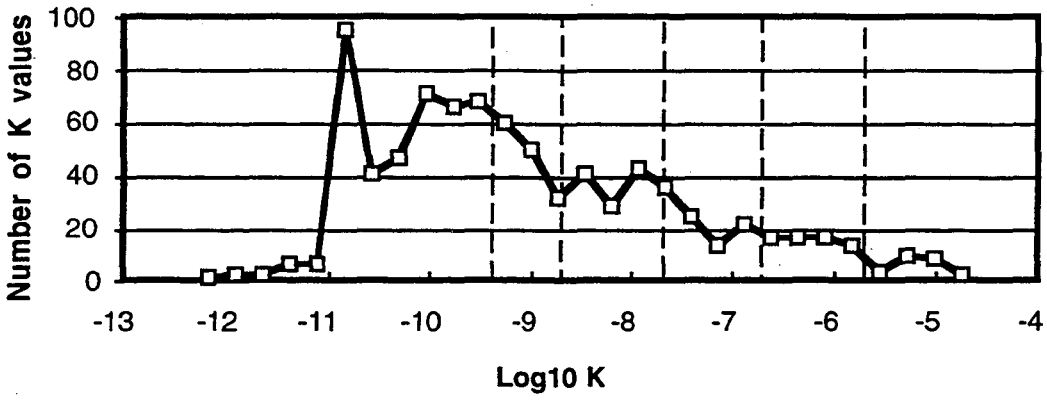

Figure 1. Frequency distribution and cumulative distribution of the "point" measurements of hydraulic conductivity as derived from injection tests in 3 m packed sections, indicators are vertical dashed lines.

In Figure 1 is shown the distribution of measured hydraulic conductivity, divided into six classes bounded by five selected thresholds or "indicators", each class spanning about an order of magnitude. The covariance structures of the K's are determined by computing the variograms for each of the six classes of the hydraulic conductivities. The computed variogram for all classes display almost a pure nugget behavior with very short correlation lengths.

The indicator covariance function is defined in terms of joint probability of two values in space:

$$E\{I(x;z_o)I(x';z_o')\}=P\{Z(x)\le z_o, Z(x')\le z_o'\} \quad . \qquad (3)$$

The expected value of the product of indicators (3) defined for the same threshold z_o is a measure of the probability that two points separated by a certain vector $\mathbf{x}$ - $\mathbf{x}'$ be jointly below the same threshold z_o. Generally, a high value of this probability implies a high

probability that the two points are connected by a range of values below the given threshold z_o. The definition of covariance in (3) makes it possible to assign a different range on connectivity for the extreme classes. If the class of the highest conductivities are given a large correlation length, the generated field can have long range connectivity for only these extreme values of large hydraulic conductivity. Regional and site geological investigations, borehole geophysical and hydrological data, and the pumping interference tests all suggest that there are extensive fractures or fracture zones on the island of Äspö. One may hypothesize that the fractures and fracture zones are actually the preferred planes where the large hydraulic conductivities are concentrated, and therefore the large conductivities will have long range connectivity within the planes of preferred orientations. The "soft" data of geological structures are incorporated in the generation of 3D stochastic field as follows: 1) assign two principal axes of anisotropy to be in the plane of a "known" fracture zone (axes Y′ and Z′), and the third axis X′ to be normal to the plane of known fracture, 2) for all except the highest class, give short correlation length along all three principal axes as indicated by the "nugget" effect of the calculated conductivity variograms, and 3) for the highest class of conductivity, assign a large correlation length in the Y′ and Z′ directions, but retain the short correlation length in the X′ direction.

Site data including surface manifestations, fracture logs and borehole radar measurements reveal extensive structures along NE, NNE, NNW (Tirén, 1993). Since the indicator simulator ISIM3D can simulate connectivity for extreme class in only one preferred plane, we constructed the hydrological model by superposing stochastic fields, each generated by ISIM3D with a different preferred plane. For reference case, we hypothesize only two preferred orientations: NNW (dip 80° to the NE) and NNE (dip 80° to the NW). Two fields were generated separately, one with the NNE preferred orientation, and the other with the NNW preferred orientation. In each generation, short, isotropic correlation length of 20 m is given to all except the highest two classes of hydraulic conductivities (which constitute 11% of all measurements). For the top 11% of conductivity, long correlation length of 200 m is assigned to the two principal axes within the plane of preferred orientation, while a short correlation length of 20 m is retained for the third principal axis normal to the preferred plane. The resultant stochastic fields having both planes of preferred orientation is obtained by superposition: 1) using values from either field at random (i.e. equal probability for each), unless 2) a value from the highest two classes occurs in one of the fields, then the value in the highest classes will be used. By construction, the superposition scheme preserves all the conditioning data; it was also found that the resultant field by superposition matches excellently the statistics of the input data. Given the inputs of the conditioning measured data and the indicator covariance structure, the simulation program ISIM3D generates hydraulic conductivities for a 3D grid of nodes within a rectangular block of $700 \times 500 \times 600$ m deep. In Figure 2 the conditioning data of measured hydraulic conductivities are shown, matched to the six classes of hydraulic conductivities distribution shown in Figure 1 by color codes, starting with the highest class in red, and descending in the colors orange, yellow, green, blue and purple. The short orange lines bracketing small sections of the boreholes represent locations of water bearing fractures from spinner tests (Stanfors et al., 1991). The orthogonal axes are easting (light blue axes) and northing (light green axes) in the local coordinates, where the local north is 11.6° counterclockwise from the true compass north as represented by the white arrow in Figure 2. Figures 3 and 4 show two views of a generated stochastic field of hydraulic conductivities for a particular realization. They are 2D photographs from the 3D pictures generated by AVS (Advance Visualization System), which allows rotation of the 3D rendition on the computer screen for views of the 3D picture from different angles. The

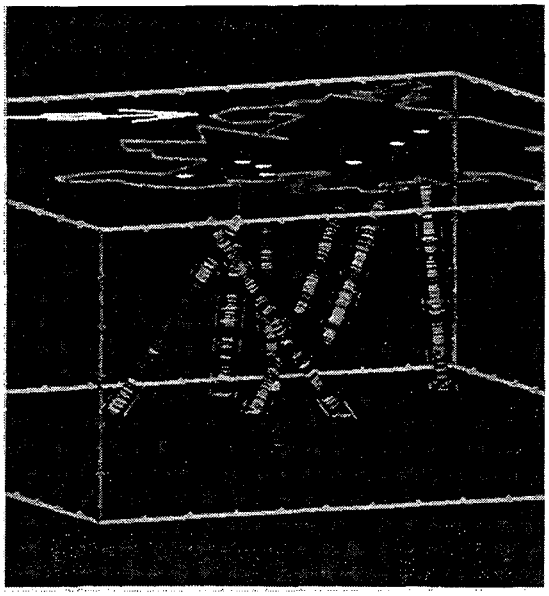

Figure 2. Conditioning data from "point" measurements of 3 m injection tests in boreholes KAS02 through KAS08.

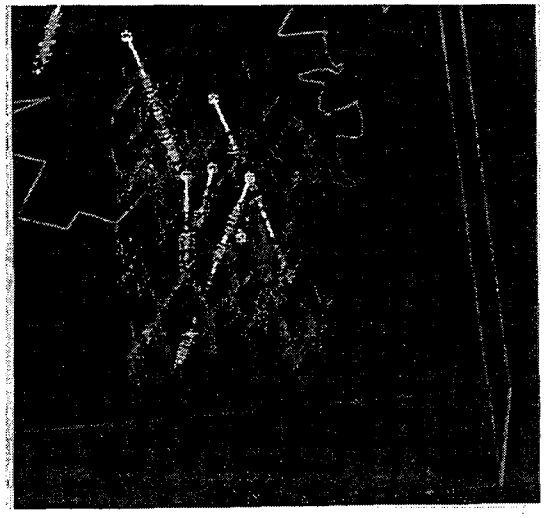

Figure 3. Location of highest class of hydraulic conductivities (red dots) for a stochastic conditioned field of K with long correlation lengths in orientations NNE and NNW.

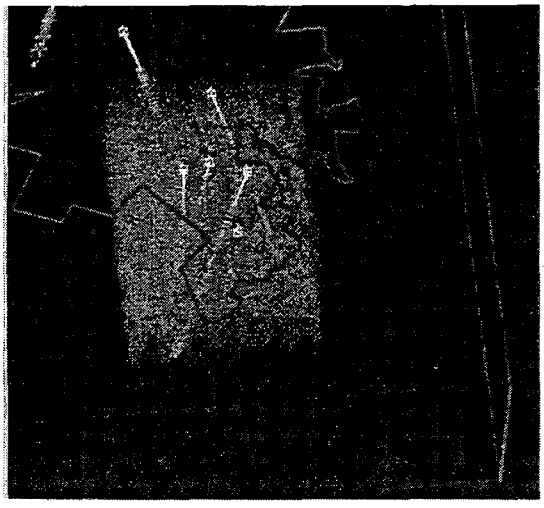

Figure 4. Location of two lower classes of hydraulic conductivities (green and blue dots) in a conditioned simulation of stochastic field.

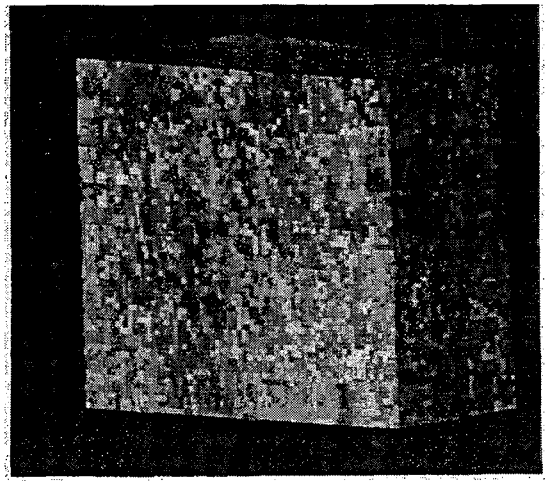

Figure 5. Stochastic field of hydraulic conductivities, highlighting a particular fracture plane.

view from an angle that the long range connectivity of high hydraulic conductivity in the NNE and NNW orientations are apparent is shown in Figure 3, where every node with a value which falls into the highest class is represented by a red dot. The long range connectivity along special orientations is absent for other classes of K, as illustrated in Figure 4 which gives only the locations of two lower classes of K (green and blue dots). The generated field of heterogeneous conductivity therefore give rise to a 3D continuum with the highest 11% of the conductivities congregating in the NNE and NNW orientations. Figure 5 shows the orthorhombic block of generated field with one slice of the preferred plane

exposed, where it can be seen the long range connectivity of the highest conductivities in red, as well as the presence of all classes of lower conductivities within the exposed plane. The fracture is therefore not represented, in our stochastic model, by a plane of constantly high conductivities in red, as it would be in a discrete fracture network model.

Steady state flow calculation may be carried out for each realization of the generated stochastic field of hydraulic conductivities. Let us consider a schematic case (Figure 6) of upward flow from the repository at the bottom, subjected to constant hydraulic head boundary conditions imposed for the top and bottom XY planes separated by 600 m, and no flow closed boundary conditions imposed on the other four faces of the 3D block. The flow region is discretized into nodes of volume $10 \times 10 \times 10$ m^3. For steady state flow, the mass balance in each node i may be written as:

$$\sum_j Q_{ij} = \sum_j K_{ij} A_{ij} \frac{(h_i - h_j)}{\Delta l_{ij}} = 0 \qquad (4)$$

where Q_{ij} is the volumetric flow from node i to j, K_{ij} is the hydraulic conductivity, and Δl_{ij} and A_{ij} are respectively the distance and interfacial area between nodes i and j. Except for the nodes that are at the boundaries where the hydraulic head is prescribed, the system of equations 4 with the hydraulic heads h_i as unknowns is solved using a conjugate gradient iterative solver. Then the steady state volumetric flow Q_{ij} and the steady state darcy velocity $v_{ij} = Q_{ij}/A_{ij}$ at the interface from node i to j are calculated. For solute transport, the velocity at any point within the $10 \times 10 \times 10$ m^3 node is linearly interpolated from the six interface v_{ij}'s. The residence time for tracer transport is obtained by particle tracking method. The particles are allowed to move in small steps along the stream lines of the velocity field and the time of travel is summed. By the above procedure, no numerical dispersion is introduced in the particle tracking scheme.

Relationship Between Heterogeneity Structure and Tracer Breakthrough

Consider an uniform source of tracer release from the bottom XY plane in Figure 6. Due to heterogeneity, flow will be strongly channeled and tracer breakthrough would have strong spatial dependence. Let the top XY plane of 500×700 m^2 be partitioned into tracer collection areas of 100×100 m^2 each. Thus the top plane is divided into 5×7 collection areas. Figure 7 show the 35 breakthrough curves from the respective collection areas, all on the same scale, with the horizontal axis for tracer arrival time and the vertical axis for fraction of collected tracer mass. Note that most breakthrough curves have multi-peak structure and vary greatly from area to area. Simulations based on different realizations give qualitatively similar results as Figure 7 in that majority of mass return are concentrated in a small fraction of the outflow area. The extreme spatially variability of the tracer breakthrough underlines that it would be unwise to base the prediction of the repository performance on the tracer breakthrough from a particular "small" area. In other words, single "point" measurements would be an inappropriate choice for the performance measure on which to base management decision. Alternatively one can examine the tracer breakthrough from the entire collection area of 500×700 m^2. The results for two different correlation structures are shown in Figure 8. The two curves on the right correspond to breakthrough from two different realizations of stochastic field with long range correlation structure for the large hydraulic conductivities in the NNW and NNE orientations. The two curves on the left correspond to stochastic fields where no long range correlation structures were assumed at all for any class of hydraulic conductivities.

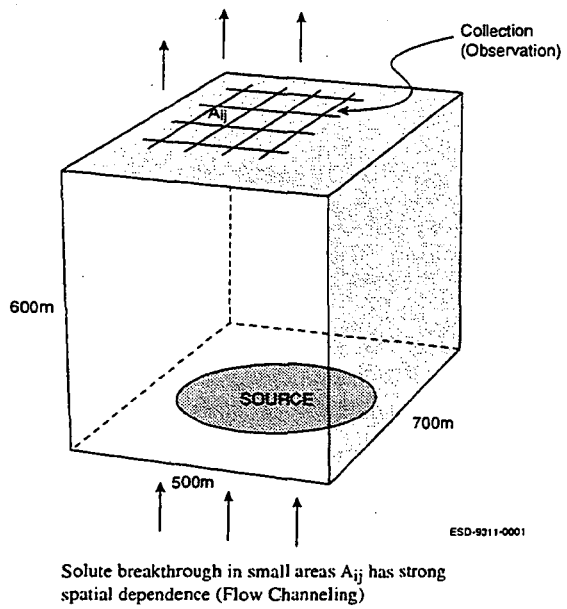

Solute breakthrough in small areas A_{ij} has strong spatial dependence (Flow Channeling)

Figure 6. Schematic diagram of flow from bottom to top in an orthorhombic block with closed boundaries on the four side.

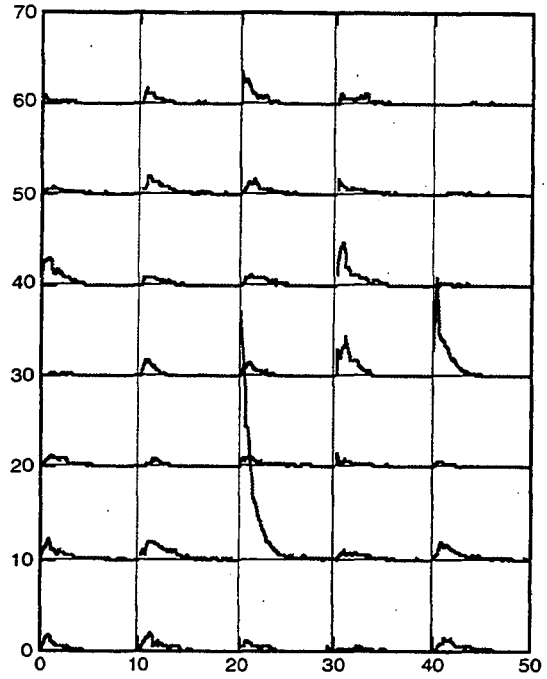

Figure 7. 35 breakthrough curves from contiguous 100×100 m^2 outflow areas in the top XY plane.

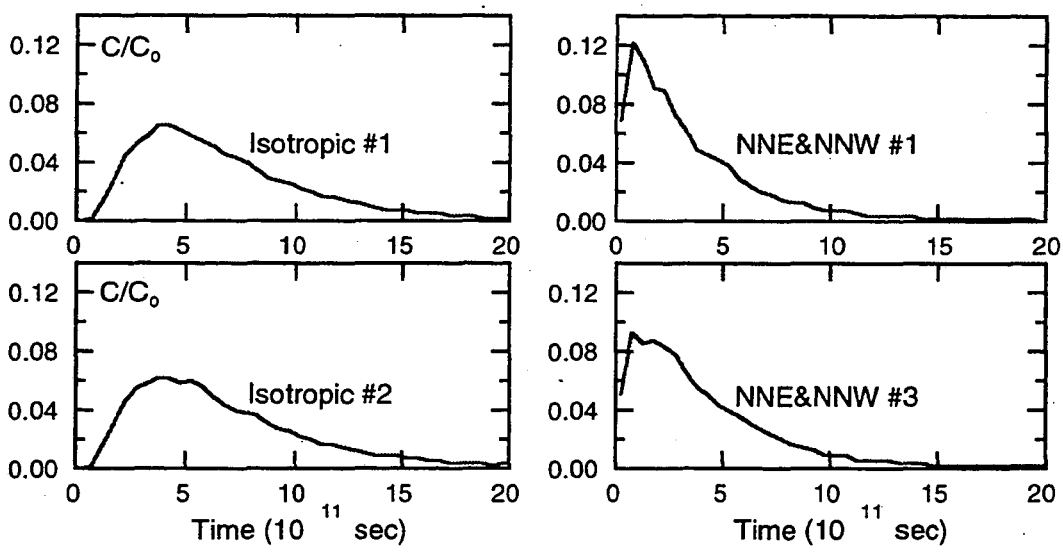

Figure 8. Spatially integrated tracer breakthrough curves for four different stochastic fields of hydraulic conductivity, conditioned on the same "point" measurements and obeying an indicator distribution of six classes with five indicators.

All four stochastic fields are conditioned to the same measured hydraulic conductivities in Figures 1 and 2. The four breakthrough curves are plotted on the same scale. It is apparent that all four curves give similar orders of magnitude in solute arrival time and concentration. The curves on the right give a slightly earlier first arrival and longer tail, since they

have long range correlation structures (fracture zones), resulting in stronger channeled flow. On the other hand, those in the left arise from transport in heterogeneous continuum with uniformly short range correlation structure for all hydraulic conductivities. Similar simulations such as those in Figure 7 carried out for these stochastic fields of Figure 8 show indeed that the tracer arrival is more evenly distributed in the 35 100×100 m^2 sampling areas for those with the isotropic correlation structure. So one may discriminate the different correlation structures by means of extensive spatial measurements such as those in Figure 7. On the other hand, when the measured data were plotted in the spatially integrated form of Figure 8, the breakthrough curves are no longer sensitive to alternative heterogeneous structures as long as all have the same set of conditioning "point" measured data. This implies that while "point" data are strongly varying, spatially integrated parameter may provide more stable and hence meaningful performance measures on which to base performance assessment predictions.

Inference From Small Scale Testing to Large Scale and Long Term Predictions

To investigate how results from site investigation measurements may be utilized for performance predictions, we hypothesized an idealized measuring scheme as shown in Figure 9. Within the same site flow geometry from bottom to top, the site investigation measurements may be a natural gradient test within a cubic volume, with tracer input over a horizontal area of 100×100 m^2, and measurements of breakthrough for transport distance of 20, 40, 60, 80, and 100 m, collected also over an area of 100×100 m^2. Whereas transport in a homogeneous medium results in breakthrough curves which can be unambiguously characterized by the mean arrival time and dispersivity; transport in heterogeneous medium gives rise to breakthrough curves which are typically multi-peaked and take on a wide range of shapes (cf Figure 7). This requires us to define empirical parameters to characterize them. In a natural gradient tests as illustrated in Figure 9, the input tracer is not expected to be fully recovered in the 100×100 m^2 collection areas, and the longer the transport distance, the less tracer shall be recovered. In making measurements, one may wait long enough until the tail of the breakthrough curve is sufficiently well defined, extrapolate the tail and estimate by integration the total mass M that would be recovered if one could wait to infinite time. We define the first parameter to be the time when half the mass has arrived, $t_{.5M}$, and the second parameter as $d_M=(t_{.8M} - t_{.2M})/t_{.5M}$, which is an empirical measure of the spread of the breakthrough. For a homogeneous medium, d_M bears a one-to-one correspondence with the inverse Peclet number. The choice of median time $t_{.5M}$ instead of the usual mean residence time attempts to minimize the effect of the very long tail on the breakthrough curve. Similarly, the choice of .8M and .2M rather than .9M and .1M in the definition of d_M is intended to avoid undue weight of the two extreme ends of the breakthrough curves. Because of the spatial variability of transport in heterogeneous medium, the numerical experiments of small scale natural gradient tests are carried out in 100 randomly chosen locations in order to arrive at the "average" parameters, as well as the range or uncertainties of parameter values. In other words, from the 100 numerical experiments, one would get 100 $t_{.5M}$ and d_M for each transport distance, from which one can order them and obtain the median, and any percentile value. For example the values corresponding to the 5^{th} and 95^{th} percentiles would give the parameter range of 90% confidence level. In Figure 10 are plotted the median values of $t_{.5M}$ and d_M at transport distances up to 100 m of the small scale experiments, as well as the parameter values for the full scale transport over 600 m transport distance with the tracer input over the entire bottom plane of 500×700 m^2. The results show that

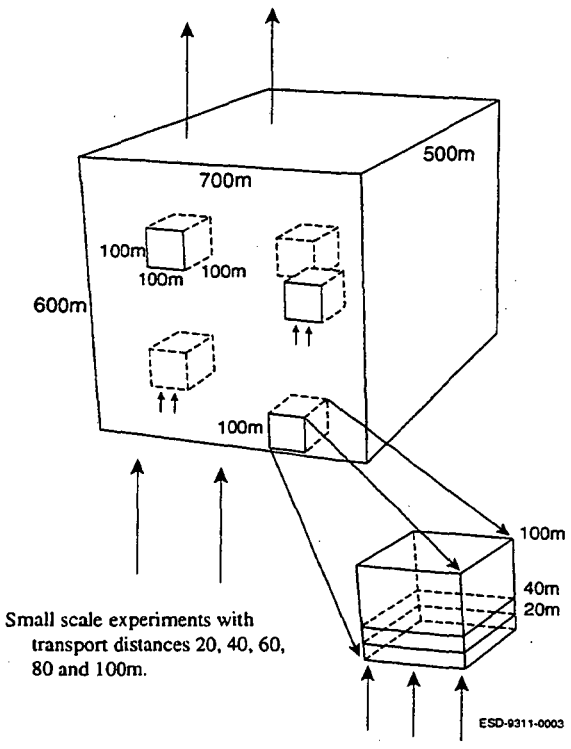

Figure 9. Schematic diagram of small scale natural gradient transport measurements within the $500 \times 700 \times 600$ m^3 orthorhombic block.

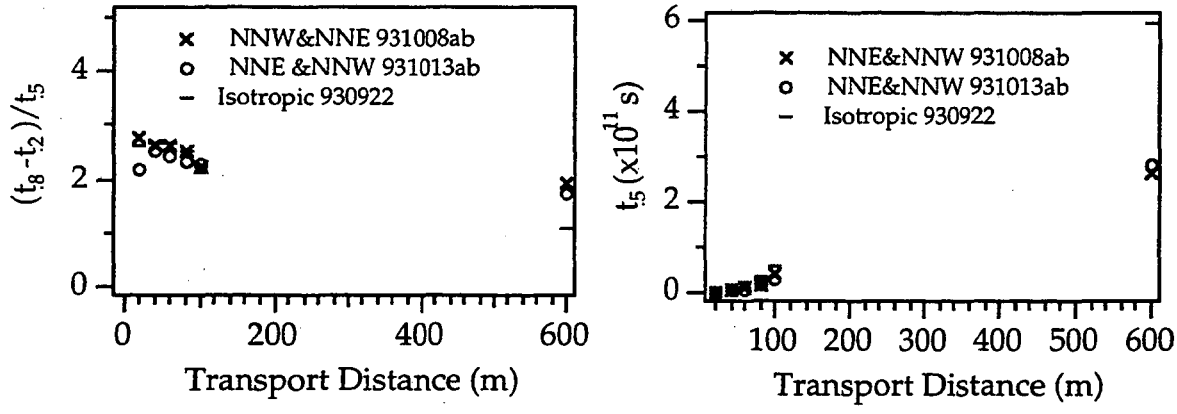

Figure 10. Median values of parameters $t_{.5M}$ and d_M for small scale measurements and the corresponding values for full scale 600 m transport.

d_M is rather stable with respect to transport distance. The slight decrease with transport distance can be understood with respect to the relationship between the transport distance of measurement and the relevant correlation length of the stochastic heterogeneous medium, which in this case is 20 m except that in certain given directions it is 200 m for the highest conductivities. Our results indicate the long range correlation of a small percentage of high conductivities does not play a significant role in affecting the dispersion of these breakthrough curves. Contrary to the invariability of d_M, the parameter $t_{.5M}$ span a large range of values with transport distance, so an linear interpolation of $t_{.5M}$ from small scale measurements underpredicts the large scale values, particularly for the isotropic system. The calculated data in Figure 10b do not falls on a straight line partly because of

the definition of $t_{.5M}$, where M decreases with transport distance in the small scale experiments. If one redefine the parameter to be $t_{.5m}$ where m is the actual total input mass, simulated results are still not linear with distance, though the deviation is smaller, indicating that for the particular case studied, the transport velocity in a heterogeneous medium is not constant under an overall uniform hydraulic gradient.

Conclusions

For a heterogeneous system, the road from site characterization (where measurements are understood and analyzed) to performance assessment (where the long term behavior of the repository is predicted) is not at all straightforward and well defined. This paper is a first attempt to address this issue. Our analyses underline the importance of choosing "proper" or meaningful performance measures. The fallibility of using "point" predictions and single measurements were demonstrated. We recommend spatial average quantities as well as a stochastic approach of multiple realizations to estimate the uncertainty. In addressing the problem of extrapolation from small scale results to long term performance, our results show that for our reference case, extrapolation from small scale results seem feasible. Good estimation of d_M and rather conservative estimates of travel time were obtained. These conclusions depend on the definitions of the parameters chosen to characterize the transport breakthrough. Our choice of a natural gradient measurement over an integrated area of 100×100 m^2, and the definition of median arrival time $t_{.5M}$ and d_M were deliberately designed to minimize variability between realizations and thus reduce uncertainty in the predictions. Different choices of experiment design and parameters can yield variable results for strongly heterogeneous media.

Acknowledgments

We would like to thank Johan Andersson and Bjorn Dverstorp for discussions, and Frank Hale for assistance in computations. Review and comments by Drs. A. D. Gupta and K. Karasaki of Lawrence Berkeley Laboratory are gratefully acknowledged. The work is jointly supported by the Swedish Nuclear Power Inspectorate (SKI) of Sweden and the Power Reactor and Nuclear Fuel Development Corporation (PNC) of Japan. The latter support is through the DOE-PNC Binational Cooperative Agreement, PNC-LBL Annex, under the auspices of U.S. Department of Energy Contract No. DE-AC03-76SF00098.

References

Gómez-Hernández, J.J. and R. M. Srivastava, 1990. ISIM3D; An ANSI-C three-dimensional multiple indicator conditional simulation program, Computers and Geosciences Vol. 16, No. 4, p. 395-440.

Stanfors, R., M. Erlström, M., I. Markström, 1991. Äspö Hard Rock Laboratory. Overview of the investigations 1986-1990., SKB Technical Report 91-20.

Tirén, S.A., P. Askling, M. Beckholmen, and S. Carlsten, 1993. A structural model of Äspö, the SKB hard rock laboratory, southeastern Sweden, Geosigma Report GRAP 93002.

Tsang , Y.W. and C.F. Tsang, 1989. Flow channeling in a single fracture as a two-dimensional strongly heterogeneous permeable medium, *Water Resources Research*, 25(9), 2076-2080.

LAWRENCE BERKELEY LABORATORY
UNIVERSITY OF CALIFORNIA
TECHNICAL INFORMATION DEPARTMENT
BERKELEY, CALIFORNIA 94720